D53

N79-24054

A COMBINED SPACECRAFT CHARGING AND PULSED X-RAY SIMULATION FACILITY*

Steven H. Face, Michael J. Nowlan,
William R. Neal, and William A. Seidler+
Spire Corporation

SUMMARY

A spacecraft charging simulation facility has been constructed to investigate the response of satellite materials in a typical geomagnetic substorm environment. The conditions simulated include vacuum, solar radiation, and substorm electrons; in addition, a nuclear threat environment simulation using a flash x-ray generator is combined with the spacecraft charging facility. Results obtained on a solar cell array segment used for a preliminary facility demonstration are presented with a description of the facility.

INTRODUCTION

Recently, much interest has been shown in the subject of anomalous behavior of electrical systems deployed in satellites in geosynchronous orbit (refs. 1-4). This behavior is now being investigated extensively in the belief that it is caused by electrostatic charging of dielectric surfaces due to the space environment (refs. 5-8). The electrical discharges associated with spacecraft charging result in electromagnetic interference which can couple into the spacecraft harness. In addition, the dielectric surface becomes contaminated with surface tracks which may lead to device failure or poor performance (ref. 9).

An electron charging facility was constructed at Spire for the simulation of the low-energy plasma environment encountered in geosynchonous orbit. A flash x-ray generator was combined with the charging facility to simulate the effects of a nuclear threat environment. In this facility the response of satellite materials can be determined for any combination of x-ray, surface charging, or simulated solar radiation, taken either separately or simultaneously. Although there have been earlier studies of spacecraft charging under a variety of conditions (refs. 10-12), the simultaneous exposure of satellite dielectrics to flash x-rays and electron surface charging has not been previously reported. Figure 1 is a schematic of the major elements of the combined facility.

*This work was supported by the Defense Nuclear Agency.
+Presently at Jaycor

This paper describes the combined x-ray and electrostatic charging facility and summarizes the preliminary results obtained during irradiation of solar cell array segments deployed on Skynet satellites.

FACILITY DESCRIPTION

Flash X-Ray Source

The x-radiation used for assessing the survivability/vulnerability of solar cells and other electrical devices is produced by the SPI-PULSE™ 6000 pulsed-power electron generator operating in the bremsstrahlung mode. The anode of the field emission tube used in these experiments is a high-Z target for the conversion of electron energy to bremsstrahlung. The diode of the field emission tube consists of a 6.4-cm diameter cathode and a 7.6-cm diameter tantalum foil anode. An 8-mm diode gap spacing provides a nominal 5- to 10-ohm load impedance for the 1.5-ohm energy store. This overmatched impedance results in the diode voltage being a significant fraction of the store voltage. Since the x-ray conversion efficiency increases with electron energy, x-ray production is increased with high-impedance loads, and depending on the charge level of the energy store, photon energies of up to 280 keV can be produced.

Diode operation is monitored by recording the voltage and current produced during discharge of the energy store. Voltage on the inner conductor of the field emission tube is measured with a capacitive divider and current is determined from a resistive shunt. The voltage and current reproducibility of the diode discharge is better than ± 5 percent.

The electron beam power pulse generated by this diode configuration has a nominal width of 150 ns FWHM. The x-ray pulse produced has a width of 100 ns FWHM due to the decrease of bremsstrahlung production efficiency for low-energy electrons at the pulse. Measurement of the x-ray time history is made with a scintillator-photodiode, consisting of an EG&G SGD-100A photodiode and a Pilot B plastic scintillator rod. A gold foil calorimeter is used to measure the x-ray fluence, which, at the center of the sample mount of the charging facility, is given by

$$\phi = 2.9 \times 10^{-12} (V_o)^{4.25} \qquad (1)$$

where ϕ is the fluence in millicalories per square centimeter and V_o is the charging voltage of the pulser in kilovolts.

The x-ray fluence at the upper and lower ends of the 45° sample mount were measured as 60 percent and 170 percent, respectively, of the central fluence.

Electron Charging Source

The electron charging facility was designed to simulate the monoenergetic electron fluxes encountered in a geomagnetic substorm environment. The electron beam is produced by a standard cathode-ray tube flood gun with a maximum thermionic current output of 1 mA. The size and intensity of the electron beam is controlled by biased grids in the gun and by the three-element cylindrical lens system shown in figure 1. The electron energy in the lens is only a few hundred volts, so that shielding from stray magnetic fields is required. The electron source and lens system is raised to accelerating potentials up to 20 kV; a copper mesh is used for the electrostatic shielding of the lens region.

A parallel-mesh acceleration field region at the exit of the lens system provides the high voltage acceleration for the electrons. Components of electron velocity perpendicular to the accelerating field are negligible compared with the velocity through the exit mesh, so that beam divergence is minimal.

The test volume consists of an aluminum vacuum chamber, 20 cm in diameter by 18 cm in length, which attaches to the diode flange of the SPI-PULSE 6000 for the combined x-ray and electron irradiations. Access to the target region is facilitated by four circumferential chamber ports.

Electron intensity and uniformity are measured with a spatially resolving Faraday collector array placed at the specimen position. The collector plate is 10 cm in diameter and contains twenty 0.8-cm-by-0.45-cm collectors across a diameter. The remainder of the collector assembly is coated with cathode-ray-tube phosphor for visual observation of the electron beam while adjusting the focus.

The orientation of the current collector array in the test chamber is controlled externally by rotation of the sample-mount rod. The current collector array may be rotated 360° to sample the entire electron beam. A representative map of the initial beam uniformity obtained for a 1-nA/cm^2 peak current density is shown in figure 2 with a solar array segment. Superimposed bremsstrahlung fluence intensities, for a representative test configuration, are also shown in the figure.

During testing, electron intensity is maintained constant by monitoring the current density with four stationary current collectors near the circumference of the beam at the entrance to the test chamber and adjusting the filament current accordingly.

Measurements of the current density made at various distances from the beam entrance aperture indicate no beam divergence or convergence within the test volume. Differences in beam current density at the top and bottom of the chamber are less than 3 percent. Current density is variable up to 30 nA/cm^2 for an 8 cm diameter beam. Higher intensities are attainable with smaller diameter beams.

Specimens are mounted on a dielectric or conductive support in the center of the test chamber. The panel is mounted at a 45° angle to expose equal areas to radiation from the electron source and x-ray source. Light from a spectrally calibrated tungsten lamp is introduced through a quartz window in the back plate of the chamber. A mirror mounted on the front plate reflects the light onto the specimen surface. Light intensity is adjusted to provide 140 mW/cm^2 incident to simulate air-mass-zero solar intensity. The quartz window is also used for viewing the sample during electron charging.

Prior to specimen irradiation, the uniformity and intensity of the electron beam are measured. The test specimen is then positioned in the chamber, while the test volume is evacuated to a pressure of less than 5×10^{-5} torr. Total pump-down time is about 15 minutes.

The electron gun filament current is adjusted to provide the intensity of interest as determined by the current measured with the four Faraday collectors at the beam periphery. During the irradiation, a TREK Model 340 HV noncontacting voltage probe is used to measure the surface electrostatic potential on test specimens. This unit has a voltage resolution of 0.1 percent, with measurements relatively independent of probe-to-surface spacing. The time-response of the probe is less than 2 ms. The potential of the probe floats to that of the surface being measured, minimizing its effect upon the test environment. The probe may be manipulated from outside the test chamber using a set of external controlling rods. Position over the test surface is indicated by an x-y plotter connected to the rods. When not in use the probe is retracted into a side chamber.

FACILITY DEMONSTRATIONS

Description of Solar Cell Array

The solar cell panels used for facility demonstration testing consisted of nine 2-cm-by-2-cm cells configured in a three-by-three array. This configuration was chosen as the smallest array which might represent an actual satellite deployment geometry (i.e., the central cell is completely surrounded by other cells). The electrical circuit of the central cell was independent of the outer cells to facilitate measurement of the cell response to various environments, although it was recognized as not being a realistic configuration.

Four solar arrays, designated 4057-1, 4057-2, 4057-3, and 4057-4, were provided by Ford Aerospace and Communications Corp. from Skynet satellites. Details of the solar cell geometry are shown in figure 3. The solar cells were n-on-p silicon fabricated from 5- to 14-ohm-cm material with junction depths of 0.25 to 0.30 micrometer. Two of the test panels, arrays 4057-3 and 4057-4, had interconnected conductive coverslip coatings of indium oxide.

The four solar cell arrays were irradiated with x-rays, electrons, and solar spectrum photons. Initially, each array was irradiated with x-rays with and without incident solar light. Array 4057-2 was pulsed more than the others to observe any

cumulative effects. Each array was charged with electrons at a nominal 1-nA/cm^2 flux level. During charging, the arrays were exposed alternately to light and darkness to simulate day-night conditions. Finally, simultaneous x-ray, electron charging, and incident light exposures were provided to assess the combined effects upon cell array performance.

At the conclusion of each phase of testing, the I-V characteristics of the central cell were measured with a Spectrosun Model X25 MKII AM0 solar simulator. In addition, the solar cells were examined for signs of physical degradation after each exposure.

Solar Cell Response to X-Rays

The solar cell arrays were subjected to x-ray fluence levels of 0.07, 0.2, and 0.45 mcal/cm^2 incident upon the central cell. These levels correspond to SPI-PULSE 6000 charging voltages of 150, 200, and 250 kV and a source-to-target distance of 9 cm. The total x-ray dose delivered was 3, 4, and 6 rads (Si) at the front surface.

The ambient temperature of the test volume was recorded for each pulse. A chromel-alumel thermocouple attached to the backside of the central cell was calibrated and monitored. Output of the thermocouple indicated a maximum temperature rise of less than 1°C at the highest x-ray fluence level. This corresponds to a 0.5 percent decrease in V_{oc} and 0.1 percent increase in cell current.

A typical cell response is shown in figure 4. The x-ray energy deposition in the solar cell saturates the junction region due to creation of electron-hole pairs. The pulsewidth of the cell output is dependent on the injection level, carrier drift velocity, carrier recombination time, and load circuit. No difference was seen in the output signal when the coverslips of arrays 4057-3 and 4057-4 were grounded.

A transient I-V curve generated from the x-ray response for panel 4057-2 is compared to the AM0 curve in figure 5. No transient response was observed during simulation of daylight conditions. Heating of the test volume with the tungsten lamp produced a slight voltage decrease. No permanently adverse effects on cell performance occurred from the x-ray exposures.

Solar Cell Response to Electron Charging

The solar cell arrays were irradiated with electrons to simulate the environment encountered in a geosynchronous orbit. The nominal flux density of the electron beam was maintained at 1 nA/cm^2, while the electron energy was varied from 2 to 20 keV.

The TREK electrostatic voltage probe recorded the potentials built up on the array surface and the fiberglass substrate. Generally, the potential of the solar cell coverslips reached one-fourth to one-third of the incident electron energy, while the

fiberglass substrate at the periphery of the array charged from one-half to two-thirds of the electron energy. A typical voltage profile across the surface is shown in figure 6.

Differences in potential on the cell surfaces also caused discharges to occur among the cell coverslips or between a cell and the fiberglass substrate. For some of the testing the front contact of the center cell was grounded. In this case, potential differences between cells due to electron charging resulted in electrical discharges from the peripheral cell coverslips to the grounded contact.

The surface discharge rate and associated potential drop were recorded with the TREK probe. A discharge over the cell surface caused the potential to drop below 1 kV. Discharges to the fiberglass substrate were generally only partial, resulting in a potential drop of 2 to 3 kV. A time history of the potential over the cell surface and substrate exposed to the electron irradiation is shown in figure 7.

Not all the electrical discharges appeared in the load circuit. If the front contact of the cell was grounded, few signals were observed in the load, since the discharge could go directly to ground. For most of the testing, the cell back contact was grounded so that discharges to the front contact would appear across the load. In this mode of operation, there was generally a coincidence in the drop in potential recorded by the TREK probe and the signal recorded in the load circuit. To obtain a signal of reasonable amplitude, a 1-MΩ preamplifier was used as a load to the solar cell.

Signals of tens of millivolts were recorded during the electrical discharges. These signals reached their peak in a few milliseconds, then decayed exponentially in about 10 ms. The charge contained in the discharge signals amounted to a few tenths of a microcoulomb. This quantity represents the charge lost in a 3-kV potential drop on the cell surface, using the calculated capacitance of a cell coverslip. The corresponding energy lost in a discharge was about 1 mJ. The electrical discharge signals were of both positive and negative polarity, and, in general, were very reproducible for fixed experimental conditions.

Photographic observation of the cell electrical discharge activity was recorded with a Polaroid camera. Open shutter photographs of 5- to 10-min exposure were taken using the chamber quartz window as a view port. Evidence of electrical discharges was observed with beam voltages from 2 to 20 kV at 1 nA/cm^2 for times of several minutes. An example of the electrical discharging is shown in figure 8.

Most of the electrical arcs occurred around the central cell whose front contact was connected to ground through the load circuit. Some discharging is evident among the outer cells. The number of visible electrical arcs increases with the surface potential of the cells.

A reduced level of discharging was observed for the conductive coverslip cell arrays. The potential of the fiberglass substrate around the cells was observed to be lower by 10 to 30 percent when the coverslips were grounded.

With the tungsten lamp turned on, the electrical discharging ceased immediately for all arrays, as determined from monitoring the cell load circuit. The potential on the fiberglass substrate decayed to a few hundred volts in minutes. No evidence of electrical discharge was recorded over the substrate.

After multiple discharges, measurement of the I-V characteristics showed that panels 4057-1 and 4057-2 experienced a loss in maximum operating power of 12 percent. Panels 4057-3 and 4057-4 incurred no effective power loss as a result of charging and discharging. The I-V curves for panels 4057-1 and 4057-4 are shown in figures 9 and 10.

Two of the solar arrays were physically damaged by the electrical discharging. The central cells of panels 4057-1 and 4057-3 each had a crack develop in the coverslip. The position of the crack on both cells coincided with an observed electrical arc. These panels were irradiated for a total time of 8h and 5h, respectively, at electron energies of up to 20 keV. The other two panels, irradiated for less than 4h each, did not develop similar coverslip cracks.

Solar Cell Response to Combined Environment Exposure

All the panels were subjected to x-ray exposure during electron irradiation. Each panel was charged with a 16-kV, 1-nA/cm^2 electron beam for 1h in the dark. The panels were then pulsed with x-rays at test levels of 3, 4, and 6 rads (Si). The conductive coverslip cells were pulsed with and without the coverslips grounded.

None of the cells exhibited anomalous behavior during the x-ray pulse. The x-ray response signals were the same as observed without electron charging. There was no potential drop observed, within the time-response of the TREK probe, either on the fiberglass substrate or over the cell surface during the x-ray pulse. It is possible that there may have been a late time response or a low-amplitude response that could not be recorded with the instrumentation available.

CONCLUDING REMARKS

The spacecraft charging facility developed at Spire represents an economical and reliable simulation device. Results obtained using a three-by-three solar cell array are in general agreement with previously published results at other facilities (refs. 13 and 14). These results demonstrate the utility of using small-area samples to simulate larger area behavior.

REFERENCES

1. Fredericks, R.W.; and Scarf, F.L.: (1973) Observations of Spacecraft Charging Effects in Energetic Plasma Regions. Photon and Particle Interactions with Surfaces in Space, R.J. Grard, ed., D. Reidel Publishing Co., Dordrecht, Holland, pp. 277-308.

2. McPherson, D.A.; Cauffman, D.P.; and Schober, W.: (1976) Spacecraft Charging at High Altitudes: The Scatha Satellite Program. Spacecraft Charging by Magnetospheric Plasmas. Progress in Astronautics and Aeronautics, Vol. 47, A. Rosen, ed.. AIAA, MIT Press, 1976, pp. 15-30.

3. Inouye, G.T.: Spacecraft Charging Anomalies on the DSCS 11, Launch 2 Satellites. Proceedings of the Spacecraft Charging Technology Conference, NASA TMX-73537, 1976, pp. 829-852.

4. Robbins, A.; and Short, C.D : Space Environmental Effects on the SKYNET 2B Spacecraft. Proceedings of the Spacecraft Charging Technology Conference, NASA TMX-73537, 1976, pp. 853-863.

5. Whipple, E.C.: Modelling of Spacecraft Charging. Proceedings of the Spacecraft Charging Technology Conference, NASA TMX-73537, 1976, pp. 225-235.

6. Rosen, A.: (1975) Spacecraft Charging - Environment Induced Anomalies. AIAA paper 75-91, AIAA 13th Aerospace Sciences Meeting, Pasadena, California.

7. Katz, I.; Parks, D.E.; Wang, S.; and Wilson, A.: Dynamic Modelling of Spacecraft in a Collisionless Plasma. Proceedings of the Spacecraft Charging Technology Conference, NASA TMX-73537, 1976, pp. 319-330.

8. Pike, C.P.: (1975) A Correlation Study Relating Spacecraft Anomalies to Environmental Data. Spacecraft Charging by Magnetospheric Plasmas. Progress in Astronautics and Aeronautics, Vol. 47, A. Rosen, ed., AIAA, MIT Press, 1976, pp. 45-60.

9. Stevens, N.J.; Lovell, R.R.; and Gore, V.: (1975) Spacecraft Charging Investigations for the CTS Project. NASA TMX-71795.

10. Keyser, R.; and Swift, O.: Analysis and Tests of a Satellite Model in a Photon Environment. IEEE Transactions on Nuclear Science NS-24, No. 6, 1977, pp. 2440-2444.

11. Luft, W.: Radiation Effects on High Efficiency Silicon Solar Cells. IEEE Transactions on Nuclear Science NS-23, No. 6, 1976, pp. 1795-1802.

12. Kalma, A.H.; and Fischer, C.J.: 4 Space Radiation of Solar Cells. IEEE Transactions on Nuclear Science NS-23, No. 6, 1976, pp. 1789-1794.

13. Stevens, N.J.; Berkopec, F.D.; Staskus, J.V.; Blech, R.A.; and Narciso, S.J.: Testing of Typical Spacecraft Materials in a Simulated Substorm Environment. Proceedings of the Spacecraft Charging Technology Conference, NASA TMX-73537, 1976, pp. 431-457.

14. Bogus, K.P.: Investigation of a CTS Solar Cell Test Patch Under Simulated Geomagnetic Substorm Charging Conditions. Proceedings of the Spacecraft Charging Technology Conference, NASA TMX-73537, 1976, pp. 487-501.

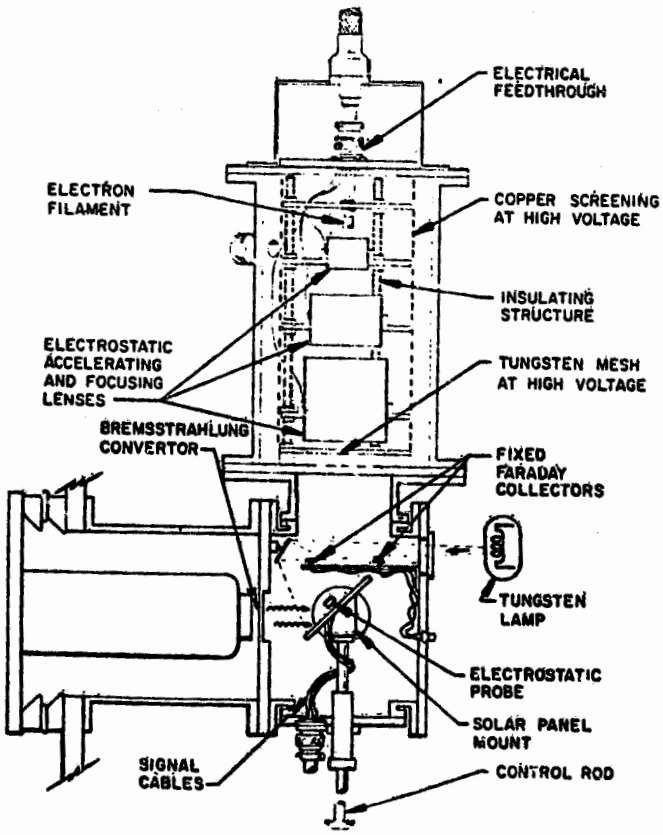

Figure 1. - Schematic of electron charging source.

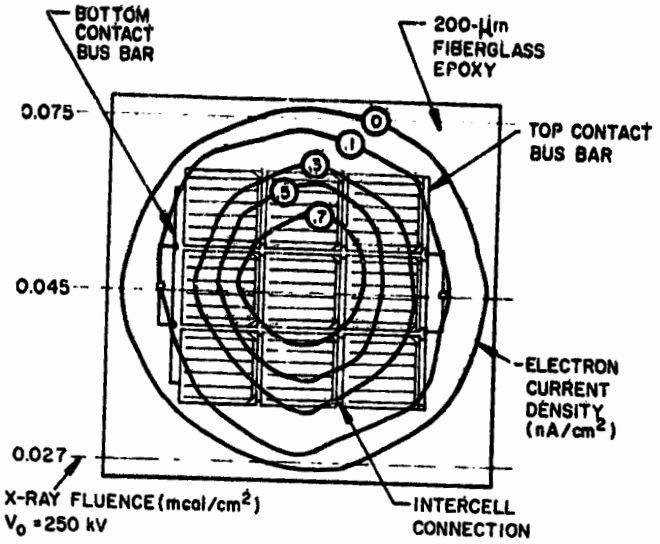

Figure 2. - Electron beam uniformity over three-by-three solar cell array.

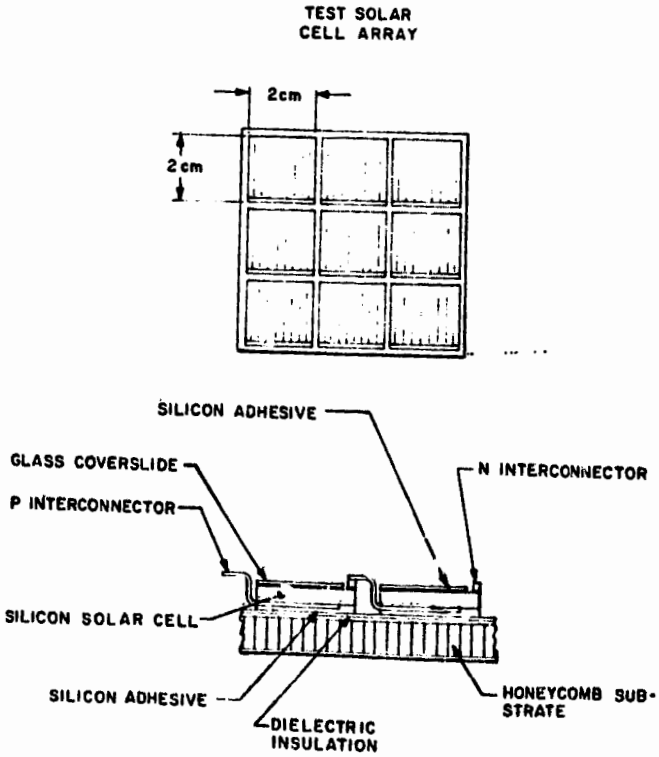

Figure 3. - Schematic of solar cell array with aluminum honeycomb substrate.

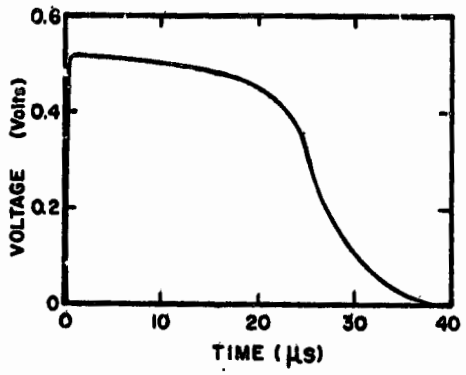

Figure 4. - Representative transient response of central cell of solar array 4057-2 to X-ray irradiation (V_0 ~ 200 keV).

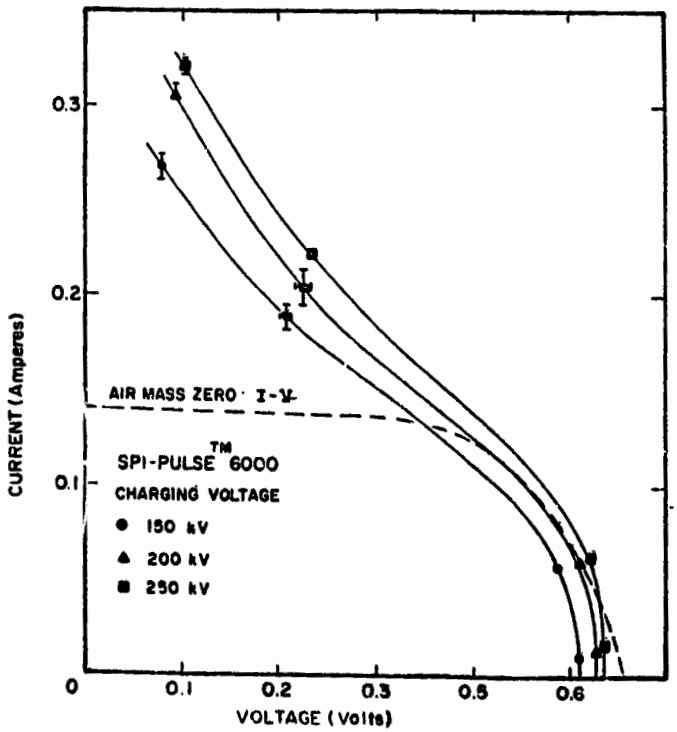

Figure 5. - Transient current-voltage characteristics of central cell of solar array 4057-2 under X-ray irradiation.

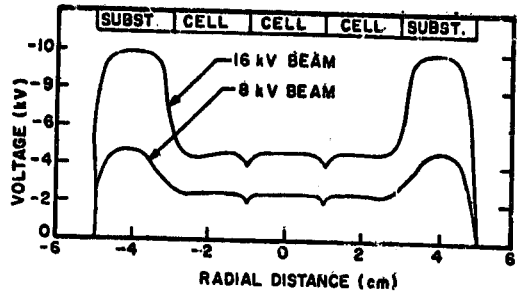

Figure 6. - Surface potential of solar array 4057-4 due to electron irradiation.

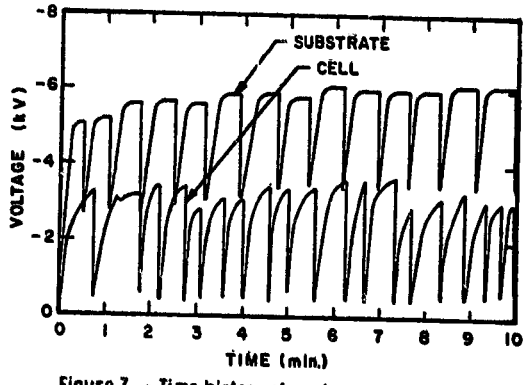

Figure 7. - Time history of surface potential of solar array 4057-4 for 16-keV electron irradiation, coverslips grounded through 1 MΩ.

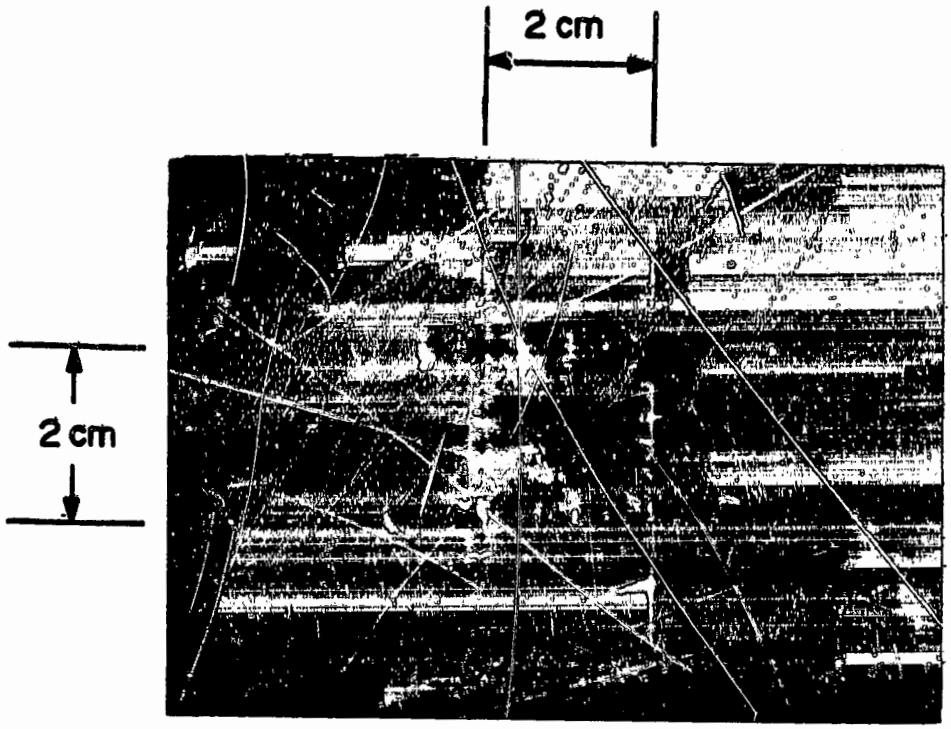

Figure 8. - Open-shutter photograph of electrical discharging of solar cell array.

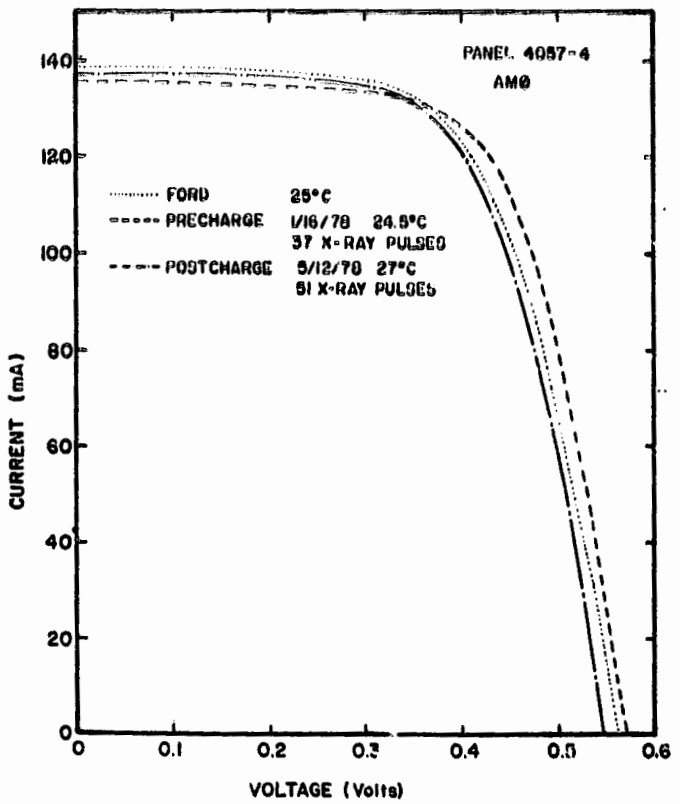

Figure 9. - Current-voltage curves for central cell of solar array 4057-4.

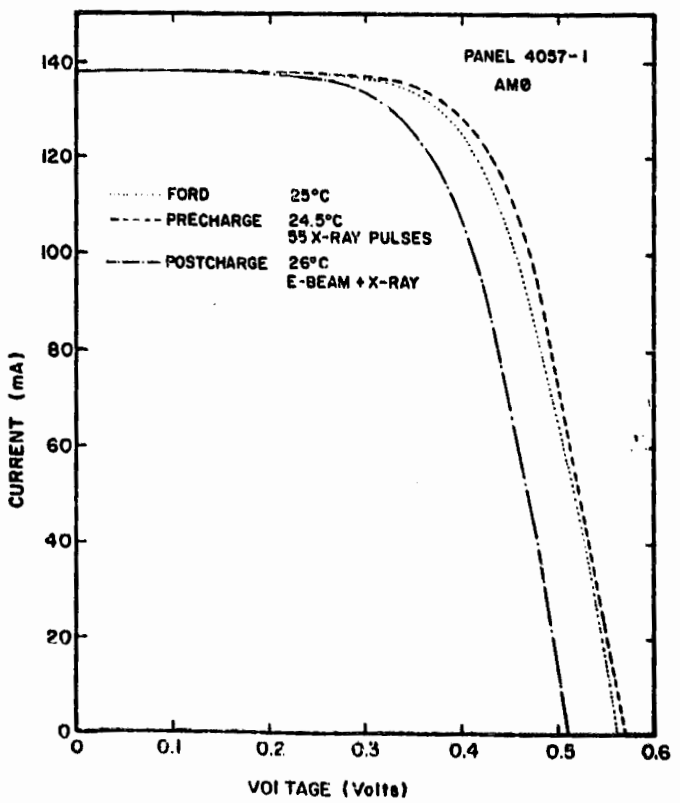

Figure 10. - Current-voltage curves for central cell of solar array 4057-1.